Solid State Nuclear Magnetic Resonance 65 (2015) 41–48

Contents lists available at ScienceDirect

Solid State Nuclear Magnetic Resonance

journal homepage: www.elsevier.com/locate/ssnmr

An NMR crystallography study of the hemihydrate of 2′, 3′-*O*-isopropylidineguanosine

G.N. Manjunatha Reddy [a], Daniel S. Cook [b], Dinu Iuga [a], Richard I. Walton [b], Andrew Marsh [b], Steven P. Brown [a,*]

[a] Department of Physics, University of Warwick, Coventry CV4 7AL, UK
[b] Department of Chemistry, University of Warwick, Coventry CV4 7AL, UK

ARTICLE INFO

Article history:
Received 9 September 2014
Received in revised form
5 January 2015
Accepted 8 January 2015
Available online 22 January 2015

Keywords:
Guanosine
Hydrate
MAS
NMR
GIPAW
^{1}H DQ
^{1}H–^{13}C
^{14}N–^{1}H
J coupling
Dipolar coupling

ABSTRACT

An NMR crystallography study of the hemihydrate of 2′, 3′-*O*-isopropylidineguanosine (Gace) is presented, together with powder X-ray diffraction and thermogravimetric analysis. ^{1}H double-quantum and ^{14}N–^{1}H HMQC spectra recorded at 850 MHz and 75 kHz MAS (using a JEOL 1 mm probe) are presented together with a ^{1}H–^{13}C refocused INEPT spectrum recorded at 500 MHz and 12.5 kHz MAS using eDUMBO-1_{22} ^{1}H homonuclear decoupling. NMR chemical shieldings are calculated using the GIPAW (gauge-including projector augmented wave) method; good two-dimensional agreement between calculation and experiment is observed for ^{13}C and ^{1}H chemical shifts for directly bonded CH and CH_3 peaks. There are two Gace molecules in the asymmetric unit cell: differences in specific ^{1}H chemical shifts are rationalised in terms of the strength of CH-π and intermolecular hydrogen bonding interactions.

1. Introduction

The collaborative computational project for NMR crystallography (CCP-NC, www.ccpnc.ac.uk) defines NMR crystallography as the combined use of experimental NMR and computation to provide new insight, with atomic resolution, into structure, disorder and dynamics in the solid state. Building upon pioneering work, notably by Harris [1,2] and Emsley [3], NMR crystallography of solid-state structures adopted by organic molecules is becoming a vibrant research area. In particular, calculations of NMR parameters using the GIPAW [4–7] (gauge-including projector augmented wave) method have been performed for a wide variety of organic solids [8–35].

This paper considers 2′, 3′-*O*-isopropylidineguanosine; using the notation in Ref. [25], this is referred to as Gace (i.e., for guanosine acetonide). Such guanosine derivatives are of interest because of the rich supramolecular chemistry exhibited in organic solutions, on surfaces and in the solid state [36–38], with self assembly being characterised by ^{23}Na, ^{39}K and ^{87}Rb [39–43] as well as ^{1}H, ^{13}C, ^{14}N and ^{15}N [25,44,45] solid-state NMR.

In this work, the hemihydrate, Gace.0.5H_2O, for which the crystal structure has been solved by single crystal X-ray diffraction [46] is studied. A suite of two-dimensional high-resolution ^{1}H solid-state NMR experiments [47] that are applicable at natural isotopic abundance (^{1}H–^{13}C refocused INEPT [48], ^{1}H double-quantum (DQ) MAS [49], and ^{14}N–^{1}H HMQC [50–53] experiments) and that use *J* couplings or dipolar couplings to probe through-bond C–H connectivities and through-space H–H and N–H proximities are performed. In the NMR crystallography approach, experimental solid-state NMR spectroscopy (together with powder X-ray diffraction and thermogravimetric analysis) is complemented by GIPAW calculations of NMR chemical shifts.

* Corresponding author. Fax: +44 24 761 50897.
E-mail address: S.P.Brown@warwick.ac.uk (S.P. Brown).

http://dx.doi.org/10.1016/j.ssnmr.2015.01.001

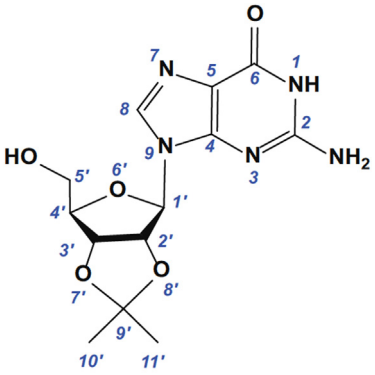

Gace

2. Experimental and computational details

Gace was purchased from Sigma-Aldrich (Gillingham, UK). PXRD data were collected at room temperature on a PANalytical X'Pert Pro MPD (Kα_1 λ=1.5406 Å) equipped with monochromatic Cu Kα_1 radiation and a PIXcel detector from a sample held in an aluminium plate. Pawley fitting of the diffraction profile was used to obtain lattice parameters—TOPAS-Academic implemented with jEdit (version 4.3.1) was employed [54]. The goodness of fit is reported as the weighted (R_{wp}) and unweighted (R_p) profile parameters, defined in the conventional way [55].

Thermogravimetric analysis was performed using a Mettler Toledo DSC1-400 instrument. ~10 mg of sample contained within a 40 μL aluminium sample pan was heated over the temperature range 25–200 °C at a constant heating rate of 10 °C per minute. A purge gas using helium was employed at a flow rate of 50 ml per minute.

Solid-state NMR experiments were performed using Bruker Avance III NMR spectrometers operating at a ^{1}H Larmor frequency of 500.1 MHz for ^{13}C–^{1}H experiments (^{13}C Larmor frequency of 125.8 MHz) or 850.2 MHz for ^{1}H and ^{14}N–^{1}H experiments (^{14}N Larmor frequency of 61.4 MHz). At 500 MHz, a Bruker 4 mm triple-resonance MAS probe (in double-resonance mode) was used, with 46 mg of Gace packed into the rotor, while at 850 MHz, a JEOL 1 mm double-resonance MAS probe was used, with 0.6 mg of Gace packed into the rotor. A recycle delay of 3 s (500 MHz) or 2 s (850 MHz) was used. In ^{13}C–^{1}H CP MAS and refocused INEPT experiments, SPINAL64 ^{1}H heteronuclear decoupling [56] with a pulse duration of 4.8 μs was applied for an acquisition time of 40 ms. The ^{1}H nutation frequency for pulses and decoupling was 100 kHz, except for ^{14}N–^{1}H experiments, where a ^{1}H 90° pulse duration of 2.0 μs was used.

^{13}C and ^{1}H chemical shifts are referenced with respect to neat TMS using adamantane as a secondary reference (38.5 ppm for the higher-ppm ^{13}C resonance [57] and 1.85 ppm for the ^{1}H resonance [58]). Experimental ^{13}C and ^{1}H chemical shifts are stated to an accuracy of ±0.1 or 0.2 ppm, respectively. ^{14}N shifts were referenced to a saturated NH_4Cl aqueous solution at −352.9 ppm, corresponding to a primary reference of CH_3NO_2 at 0 ppm. To convert to the corresponding ^{15}N chemical shift scale frequently used in protein NMR, where the reference is liquid ammonia at −50 °C, it is necessary to add 379.5 to the given values [59].

Pulse sequences and coherence transfer pathway diagrams for the ^{1}H (SQ-DUMBO)—^{13}C SQ refocused INEPT [48], ^{1}H DQ MAS [49] using BABA (back-to-back) recoupling [60,61], and ^{14}N–^{1}H HMQC [51] two-dimensional experiments are shown in Fig. 5 of Ref. [48], Fig. 7 of Ref. [62], and Fig. 3a of Ref. [51]. For the ^{1}H (SQ-DUMBO)—^{13}C SQ refocused INEPT experiment, a 16-step phase cycle was used as described in Ref. [48]. For the ^{1}H DQ MAS experiment, a 16-step phase cycle was used to select $\Delta p = \pm 2$ on the DQ excitation pulses (4 steps) and $\Delta p = \pm 1$ (4 steps) on the z-filter 90° pulse, where p is the coherence order. For the ^{14}N–^{1}H HMQC experiment, a 4-step nested phase cycle was used to select changes in coherence order $\Delta p = \pm 1$ (on the first ^{1}H pulse, 2 steps) and $\Delta p = \pm 1$ (on the last ^{14}N pulse, 2 steps). A modified version of the pulse sequence was employed [25] whereby a second ^{1}H 90° pulse (90° out of phase with respect to the first 90° pulse) was applied immediately after the first ^{1}H 90° pulse and using phase inversion (0° and 180° every rotor period) [63] of the n=2 ($\nu_1 = 2\nu_R$) rotary-resonance recoupling (R^3) [64] pulses.

For the 2D ^{1}H–^{13}C refocused INEPT experiment, eDUMBO-1_{22} homonuclear decoupling, [65,66] was employed during the ^{1}H evolution period and the τ and τ' spin-echo durations. The 32 μs eDUMBO-1_{22} cycle was divided into 320 steps of 100 ns. Pulse sequences employing ^{1}H homonuclear decoupling use pre-pulses to take into account the tilting of the effective field away from the x and y plane of the rotation frame: [67] a pre-pulse duration of 0.8 μs was used. The scaling factor was determined experimentally (by using the ^{1}H chemical shifts of the resolved resonances in a ^{1}H 75 kHz MAS spectrum) as 1.60. For ^{13}C pulses, the ^{13}C 90° pulse length was 4.0 μs.

Calculations were performed using the CASTEP code [68], academic release version 6.1. Geometry optimisations and NMR chemical shift calculations using the GIPAW [4,5] method employed the PBE exchange correlation functional [69] with a semi empirical dispersion correction scheme due to Tkatchenko and Sheffler [70]—for more details of the implementation in NMR calculations see Ref. [33]. A plane wave basis set with ultra-soft pseudopotentials [71] with a maximum cut-off energy of 800 eV was used; integrals were taken over the Brillouin zone by using a Monkhorst–Pack grid of minimum sample spacing $0.08 \times 2\pi$ Å^{-1}. Geometry optimisation was performed with the unit cell parameters fixed, starting from the X-ray single-crystal structure [46] determined at ambient temperature of Gace.0.5H_2O, CSD code VUYMIL, Z=4 (166 atoms in the unit cell), space group $P2_1$, Z'=2, i.e., two distinct isopropylidineguanosine molecules and one water molecule in the asymmetric unit cell. The forces, energies and displacements were converged to better than 0.01 eV Å^{-1}, 0.0000004 eV, and 0.001 Å, respectively. Note that distances stated in this paper are extracted from this geometry optimised crystal structure.

3. Results

3.1. PXRD and TGA

Figs. 1 and 2 present powder X-ray diffraction (PXRD) and thermogravimetric analysis (TGA), respectively, for the Gace.0.5H_2O sample. In Fig. 1, satisfactory agreement following Pawley fitting of the diffraction pattern (this corresponds to refining only the unit cell parameters, i.e., there is no consideration of the atomic coordinates within the unit cell) with respect to the published single-crystal X-ray diffraction structure [46] is observed. Table 1 compares the refined unit cell parameters to those of the published structure, showing the good agreement. By TGA (see Fig. 2), a weight loss of 2.2% is observed. The loss of half a water molecule per formula unit corresponds to 9 g/mol, i.e., 2.7% of the molecular weight of 323.3 g/mol for Gace.0.5H_2O. Thus, the experimentally observed weight loss of 2.2% is close to, but not exactly the same as, that expected for Gace.0.5H_2O.

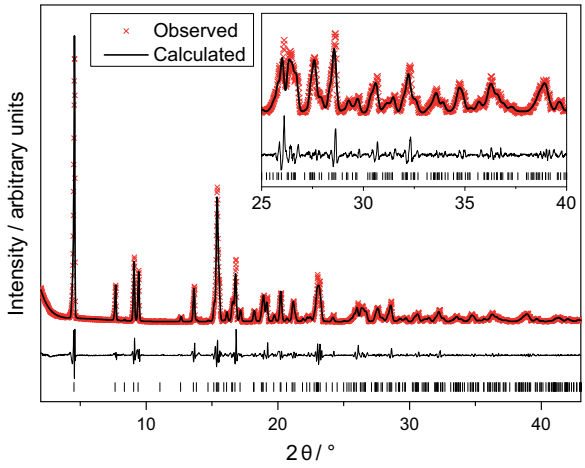

Fig. 1. Final profile fit to the PXRD pattern of the Gace.0.5H_2O sample (R_{wp}=15.10% and R_p=10.96%). The thin line is the difference trace and the tick marks denote positions of allowed Bragg reflections for the $P2_1$ unit cell (see Table 1).

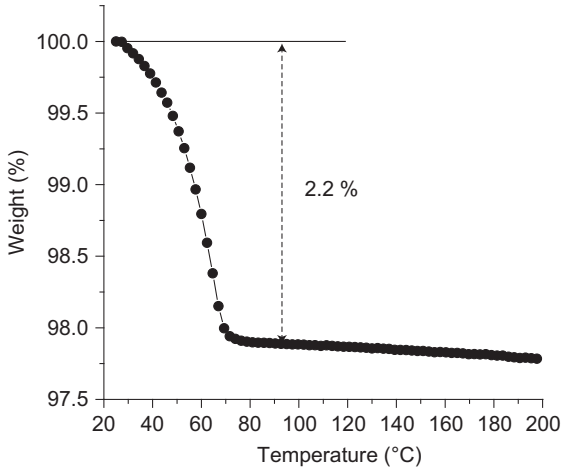

Fig. 2. Thermogravimetric analysis of the Gace.0.5H_2O sample.

Table 1
Refined lattice parameters from powder X-ray diffraction analysis (space group $P2_1$).

Lattice parameter	Lattice parameters from Mande et al. [46]	Refined lattice parameters
a (Å)	11.595(2)	11.6514(11)
b (Å)	6.757(3)	6.7816(11)
c (Å)	19.593(4)	19.6958(26)
α (deg)	90.000	90.0000
β (deg)	97.65(2)	97.6614(83)
γ (deg)	90.000	90.0000

3.2. Experimental and GIPAW calculated ^{13}C chemical shifts

Fig. 3 presents a ^{13}C CP MAS NMR spectrum of Gace.0.5H_2O. It is evident that there are more peaks than the number of distinct carbon atoms, thirteen, for example, there are two peaks at 136.0 and 137.4 ppm for C8; this corresponds to the presence of two distinct Gace molecules in the asymmetric unit cell.

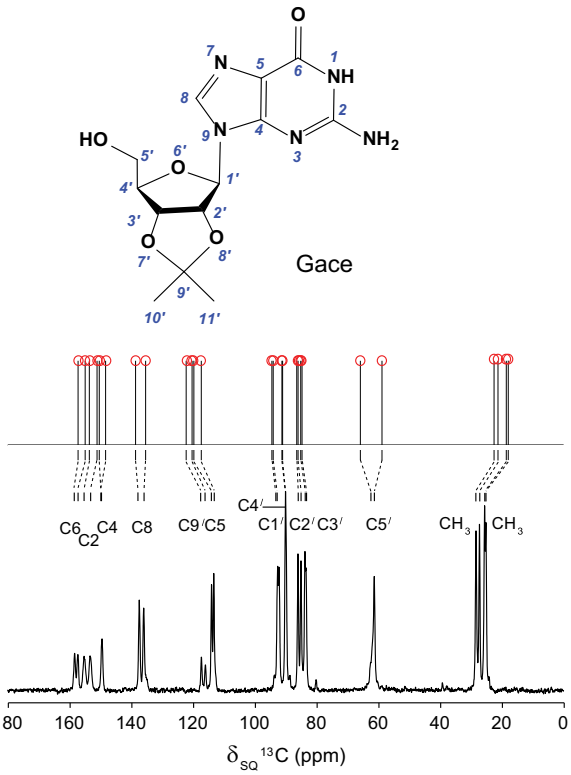

Fig. 3. ^{13}C CP MAS (12.5 kHz) of Gace.0.5H_2O recorded at a ^1H Larmor frequency of 500.1 MHz. 2048 transients were coadded, corresponding to an experimental time of 104 min. A 70–100% ramp [74] was applied on the ^1H channel for a CP contact time of 1.0 ms. The stick spectrum above the experimental spectrum corresponds to the GIPAW calculated chemical shifts (see Table 2 and Fig. 4b, using σ_{REF}=168.1 ppm) for the geometry optimised (CASTEP) crystal structure of Gace.0.5H_2O.

The NMR chemical shieldings have been calculated using the GIPAW [4,5] method for the single-crystal X-ray diffraction structure of Gace.0.5H_2O [46]. The output of such a GIPAW calculation is the absolute chemical shielding for each distinct site in the asymmetric unit cell. Table 2 lists these GIPAW calculated absolute chemical shieldings: specifically, the three tensor components in the principal axes system (labelled XX, YY and ZZ) are stated, as well as the isotropic value which is the average of the three tensor components.

Fig. 4 presents two plots of the experimental ^{13}C chemical shifts against the GIPAW calculated absolute isotropic ^{13}C chemical shieldings for the thirteen carbon atoms in the two distinct Gace molecules in the asymmetric unit cell. The plots differ in the procedure to find the line of best fit: in Fig. 4a, the (negative) gradient is allowed to deviate from unity, while in Fig. 4b, it is constrained to equal one. In both plots, the intercept with the y axis determines the reference shielding, σ_{REF}, that is used to relate calculated and experimental chemical shifts, i.e., δ_{iso}(calc)=σ_{REF}−gradient σ_{iso}(calc). In line with our previous publications [9,15,18,19,22,25,32,72,73], we adopt the convention here of constraining the (negative) gradient to equal unity; in this way, σ_{REF} is simply determined as the sum of the average experimental chemical shift and the average calculated absolute isotropic chemical shielding. In Fig. 3, the stick spectrum above the experimental ^{13}C CP MAS NMR spectrum corresponds to the calculated GIPAW ^{13}C chemical shifts for Gace.0.5H_2O; it is observed that a consequence of using this convention, i.e., constraining the (negative) gradient to equal unity, is that calculated chemical shifts are too low for the low-ppm ^{13}C resonances.

Table 2
GIPAW calculated absolute shieldings (in ppm) for the geometry optimised (CASTEP) crystal structure [46] of Gace.0.5H_2O.

Chemical site	Molecule	σ_{XX}	σ_{YY}	σ_{ZZ}	σ_{ISO}
N**H1**	A	11.68	14.22	29.81	18.57
	B	5.96	12.28	30.23	16.16
N$\mathbf{H_{2b}}$	A	14.31	19.07	34.43	22.60
	B	12.82	16.43	34.32	21.19
N$\mathbf{H_{2a}}$	A	16.52	18.08	36.53	23.71
	B	18.28	20.49	33.59	24.12
H8	A	24.04	24.81	26.02	24.96
	B	21.70	22.63	25.88	23.40
H1′	A	26.80	25.47	22.90	25.06
	B	19.96	21.71	29.24	23.63
H2′	A	20.82	24.71	29.71	25.08
	B	21.41	23.49	29.15	24.68
H3′	A	28.89	25.09	20.71	24.90
	B	19.45	22.68	31.80	24.65
H4′	A	24.52	25.28	29.24	26.35
	B	23.57	24.48	30.34	26.13
H5′$_a$	A	31.81	27.66	21.91	27.13
	B	20.68	25.16	31.73	25.86
H5′$_b$	A	21.60	26.08	30.64	26.11
	B	25.06	27.37	30.90	27.78
C$\mathbf{H_3}$	A	25.42	26.76	34.88	29.02
	B	27.44	28.38	32.25	29.26
C$\mathbf{H_3}$	A	28.01	27.93	31.48	29.14
	B	20.22	24.25	37.35	29.29
5′O**H**	A	11.13	15.00	43.41	23.18
	B	33.27	29.31	23.98	22.81
$\mathbf{H_{water}}$		12.45	16.51	43.45	24.14
		20.45	21.33	43.72	28.50
C2	A	−41.55	−1.34	93.74	16.95
	B	−36.67	−13.24	93.27	14.45
C4	A	−58.13	14.42	96.88	17.72
	B	−52.74	16.65	95.44	19.78
C5	A	11.66	18.64	120.86	50.39
	B	12.34	14.88	116.58	47.93
C6	A	87.44	25.15	−73.72	12.96
	B	81.33	29.67	−78.52	10.83
C8	A	96.12	46.40	−44.77	32.58
	B	96.80	36.51	−45.45	29.28
C1′	A	44.06	68.39	107.47	73.31
	B	44.04	69.94	107.55	73.84
C2′	A	114.68	85.53	45.35	81.85
	B	116.05	84.58	46.02	82.22
C3′	A	123.17	84.37	40.46	82.67
	B	42.21	82.37	124.29	82.95
C4′	A	40.95	71.06	117.61	76.54
	B	43.78	74.12	112.63	76.84
C5′	A	77.81	99.65	149.68	109.05
	B	72.85	98.89	134.32	102.02
C9′	A	14.84	41.97	85.40	47.40
	B	7.89	45.84	84.01	45.91
C$\mathbf{H_3}$	A	126.86	139.35	173.48	146.56
	B	122.12	136.93	176.80	145.28
C$\mathbf{H_3}$	A	128.21	141.34	178.04	149.20
	B	126.59	146.20	176.85	149.88
N1	A	−17.57	70.39	161.10	71.31
	B	−23.33	56.97	158.32	63.99
N2	A	187.17	163.24	84.53	144.98
	B	178.12	159.64	79.02	138.93
N3	A	−102.53	−1.74	237.81	44.51
	B	−55.86	19.72	224.98	62.95
N7	A	−195.78	−67.32	223.76	−13.11
	B	−200.24	−76.43	224.52	−24.05
N9	A	−10.59	13.14	134.86	45.80
	B	−23.00	14.25	134.77	42.01
O6	A	−219.19	−95.63	318.57	1.25
	B	−266.16	−119.95	322.64	−21.16
O2′	A	228.89	172.55	74.22	158.55
	B	246.55	175.43	59.12	160.37
O3′	A	213.63	160.56	74.50	149.56
	B	243.23	188.64	62.88	164.58
O5′	A	272.45	205.29	108.18	195.32
	B	229.71	179.48	72.97	160.72
O6′	A	292.11	283.80	244.90	273.60
	B	300.84	248.87	184.83	244.82
$\mathbf{O_{water}}$		258.33	278.64	331.17	289.38

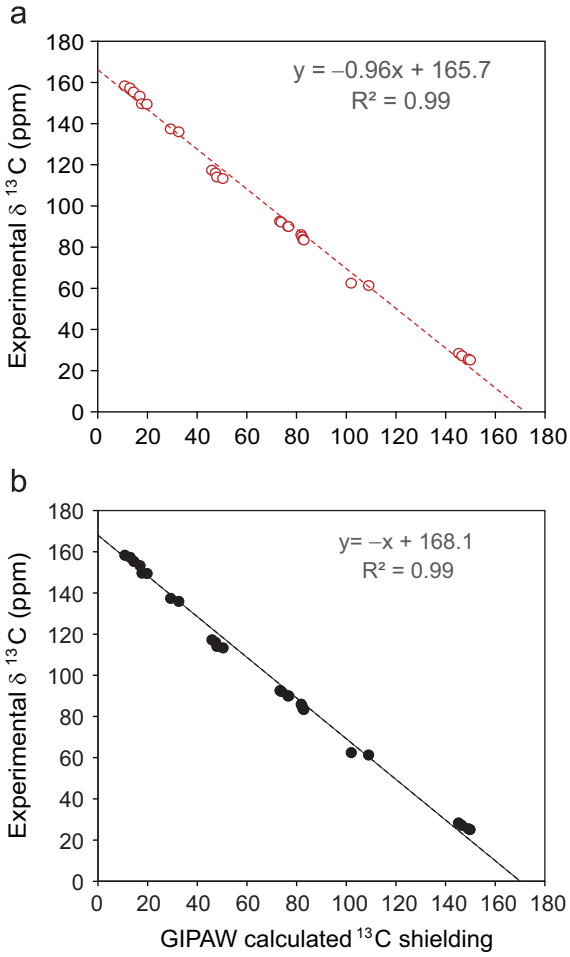

Fig. 4. Plots of the experimental ^{13}C chemical shifts (see Fig. 3) against the GIPAW calculated absolute isotropic ^{13}C shielding for the thirteen carbon atoms in the two distinct Gace molecules in the asymmetric unit cell. The line of best fit is determined by (a) allowing deviation from unity or (b) constraining the (negative) gradient to equal one.

3.3. *^{1}H–^{13}C refocused INEPT, ^{1}H DQ MAS and ^{14}N–^{1}H HMQC spectra*

^{1}H chemical shifts provide additional structural insights, for instance, information on hydrogen bonding interactions which is prominent in driving the self-assembly of guanosine derivatives. Obtaining high resolution ^{1}H NMR spectra for organic molecules in the solid state is challenging due to the presence of a network of dipolar coupled protons. Enhanced resolution can be achieved by either fast MAS or combining physical spinning under MAS with carefully synchronized rotations of the nuclear spins using radio-frequency pulses in the so-called CRAMPS (combined rotation and multiple-pulse spectroscopy) approach [47]. Moreover, the resolution and assignment of ^{1}H chemical shifts can be achieved via two-dimensional heteronuclear correlation spectra, e.g., *J*-based through-bond ^{1}H–^{13}C [48,75] and dipolar-based ^{14}N–^{1}H HMQC [50–53] spectra can be recorded at natural abundance [47].

The two-dimensional ^{1}H–^{13}C refocused INEPT [48] experiment reduces spectral complexity in the ^{1}H dimension by correlating protons with directly bound carbon atoms, and is applicable, when employing homonuclear ^{1}H decoupling, at moderate MAS frequencies. This is illustrated in Fig. 5 where the spectral regions corresponding to CH and CH_3 carbons are presented for an experiment performed at 12.5 kHz MAS using eDUMBO-1_{22} [65,66] ^{1}H decoupling and short spin-echo durations such that only cross peaks corresponding to one-bond CH connectivities are observed. Red crosses in Fig. 5 correspond to calculated ^{13}C and ^{1}H

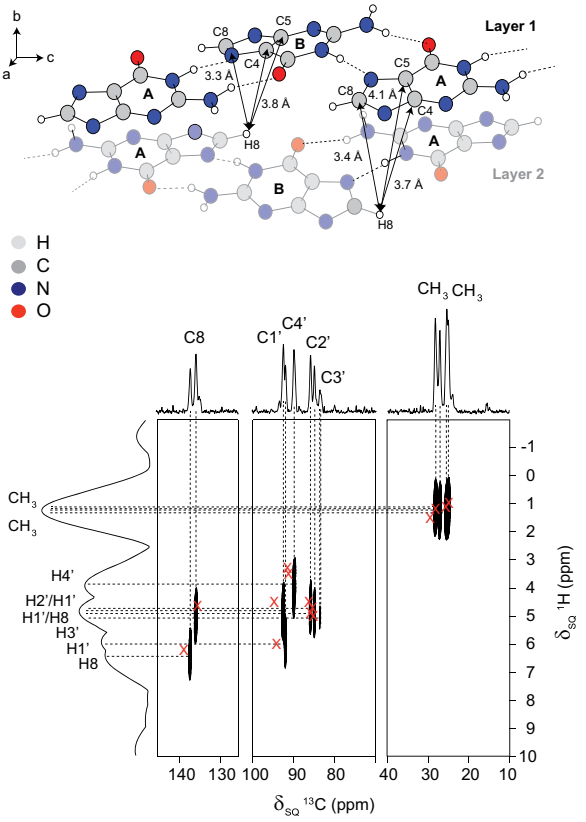

Fig. 5. A ^{1}H (500 MHz)–^{13}C refocused INEPT (12.5 kHz MAS, eDUMBO-1$_{22}$ ^{1}H homonuclear decoupling) spectrum, together with skyline projections, of Gace.0.5H$_2$O, recorded using a spin-echo duration, $\tau=\tau'=1.4$ ms. 512 Transients were co-added for each of 48 t_1 FIDs (with a t_1 increment of 80 μs, using the States-TPPI method to achieve sign discrimination in F_1), corresponding to a total experimental time of 21 h. The base contour level is at 12%. Crosses (in red) correspond to the GIPAW calculated ^{13}C and ^{1}H chemical shifts for directly bonded CH and CH$_3$ moieties (see Table 2), using $\sigma_{REF}=29.6$ ppm for ^{1}H and 168.1 ppm (125–145 ppm and 70–100 ppm regions) and $\sigma_{REF}=30.4$ ppm for ^{1}H and 174.1 ppm for ^{13}C (10–40 ppm region) for the geometry optimised (CASTEP) crystal structure of Gace.0.5H$_2$O. A schematic representation of the crystal structure (only guanine moieties are shown for simplicity of presentation) is shown above the spectrum to illustrate different CH-π interactions for the two CH8 ^{1}H environments in the asymmetric unit cell—note that the distances from H8 of molecule A to C4 and C5 of molecule B are both 3.8 Å. (For interpretation of the references to colour in this figure legend, the reader is referred to the web version of this article.)

isotropic chemical shifts for the directly bonded CH moieties; using the procedure presented in Ref. [19], the ^{13}C reference shielding is adjusted for each spectral region. It is seen that there is a good two-dimensional correlation between experiment and GIPAW calculated chemical shifts (see also Table 3), as has been observed for other organic solids [11,19,22,32,76,77]. It is noted that Czernek and Brus have presented covariance-based statistical analyses of the quality of such two-dimensional correlations between experiment and calculation [78,79].

It is interesting to comment upon the markedly different ^{1}H chemical shifts for the two H8 protons that are observed both experimentally and in the GIPAW calculations. The schematic representation of the crystal structure in Fig. 5 shows that the guanosine ribbons in Gace.0.5H$_2$O are modulated along the crystallographic *c* axis in such a way that CH-π interactions are differently experienced for H8 in the two distinct molecules in the asymmetric unit cell: distances between H8 and C4, C5 and C8 of two successive G-ribbons stacked on top of each other along the crystallographic axis *b* are stated in Fig. 5. A relatively large difference in the H1′ chemical shifts is also observed: though the base-sugar conformations of both A and B are both in a *syn*

Table 3
Comparison of calculated[e] (GIPAW) and experimental (see the ^{1}H–^{13}C correlation spectra in Fig. 5, while experimental shifts of NH1 and NH$_2$ are extracted from the ^{1}H DQ and ^{14}N–^{1}H HMQC spectra (see Fig. 7)) chemical shifts for Gace.0.5H$_2$O.

Chemical site	Molecule	^{13}C chemical shifts in ppm		^{1}H chemical shifts in ppm	
		δ_{expt}	δ_{calc}	δ_{expt}	δ_{calc}
CH_3	A	25.6	24.2[a]	1.1	1.1[c]
	B	25.2	24.9[a]	1.0	1.2[c]
CH_3	A	27.2	27.5[a]	1.1	1.3[c]
	B	28.4	28.8[a]	1.0	1.6[c]
CH8	A	136.0	135.5[b]	4.9	4.6[d]
	B	137.4	138.8[b]	6.1	6.2[d]
CH1′	A	92.6	94.7[b]	4.7	4.5[d]
	B	92.2	94.2[b]	5.7	6.0[d]
CH2′	A	86.0	86.2[b]	4.6	4.5[d]
	B	85.1	85.8[b]	4.8	4.9[d]
CH3′	A	83.7	85.4[b]	4.7	4.7[d]
	B	83.5	85.1[b]	4.9	5.0[d]
CH4′	A	90.0	91.5[b]	3.4	3.3[d]
	B	90.0	91.2[b]	3.6	3.5[d]
CH5′$_a$	A	61.4	66.0[b]	2.7	2.5[d]
	B	62.5	66.0[b]	4.0	3.7[d]
CH5′$_b$	A	61.4	59.0[b]	3.8	1.8[d]
	B	62.5	59.0[b]	2.3	2.4[d]
NH1	A			11.6	11.0[d]
	B			12.3	13.4[d]
NH_{2a}	A			5.8	5.9[d]
	B			5.7	5.5[d]
NH_{2b}	A			6.3	7.0[d]
	B			6.4	8.4[d]

[a] $\sigma_{REF}=174.1$ ppm.
[b] $\sigma_{REF}=168.1$ ppm.
[c] $\sigma_{REF}=30.4$ ppm.
[d] $\sigma_{REF}=29.6$ ppm.
[e] $\delta_{iso}(calc)=\sigma_{REF}-\sigma_{iso}(calc)$.

conformation [25], there is a marked difference in the torsional angle across the glycosidic linkage C4–N9-C1′–O6′ i.e., 72° in molecule A and 81° in molecule B.

Although the ^{1}H–^{13}C INEPT spectrum in Fig. 5 is very valuable for resolving and assigning proton resonances for hydrogens directly bonded to carbon atoms, it fails to provide information for the NH1 and NH2 sites, with it being these hydrogen atoms that exhibit intermolecular NH…*X* hydrogen bonding that drives guanosine self-assembly. It is shown here how a combination of ^{1}H DQ and ^{14}N–^{1}H HMQC spectra is a powerful probe of the environment of such NH and NH$_2$ moieties.

Fig. 6 presents a ^{1}H DQ MAS [49] spectrum of Gace.0.5H$_2$O recorded using one rotor period of BABA recoupling [60,61] at high magnetic field (^{1}H Larmor frequency of 850 MHz) and fast MAS (75 kHz using a JEOL 1 mm probe). The high resolution is sufficient to resolve many separate DQ peaks, whose assignment is indicated. Distinct cross peaks are evident even for the crowded spectral region corresponding the sugar ^{1}H resonances. It is of particular interest to consider the spectral region corresponding to the NH, NH$_2$ and H8 ^{1}H resonances; this region from the ^{1}H DQ MAS spectrum is presented at the top in Fig. 7. Fig. 7 also presents a ^{14}N–^{1}H HMQC spectrum (middle, also recorded at 850 MHz, 75 kHz MAS), wherein N–H proximities are probed using $n=2$ rotary resonance recoupling (R^3) [64] of the heteronuclear dipolar couplings [51]. A short R^3 recoupling time is used such that only one-bond NH correlations are observed [53]. The bottom two-dimensional spectrum in Fig. 7 corresponds to the C8 region of the ^{1}H–^{13}C refocused INEPT spectrum presented in Fig. 5. Note that there is ^{1}H direct detection in t_2 in the ^{14}N–^{1}H HMQC experiment as compared to ^{1}H indirect detection in t_1 in the ^{1}H–^{13}C refocused INEPT experiment—to enable a consistent presentation, the region of the ^{1}H–^{13}C refocused INEPT spectrum presented in Fig. 7 has

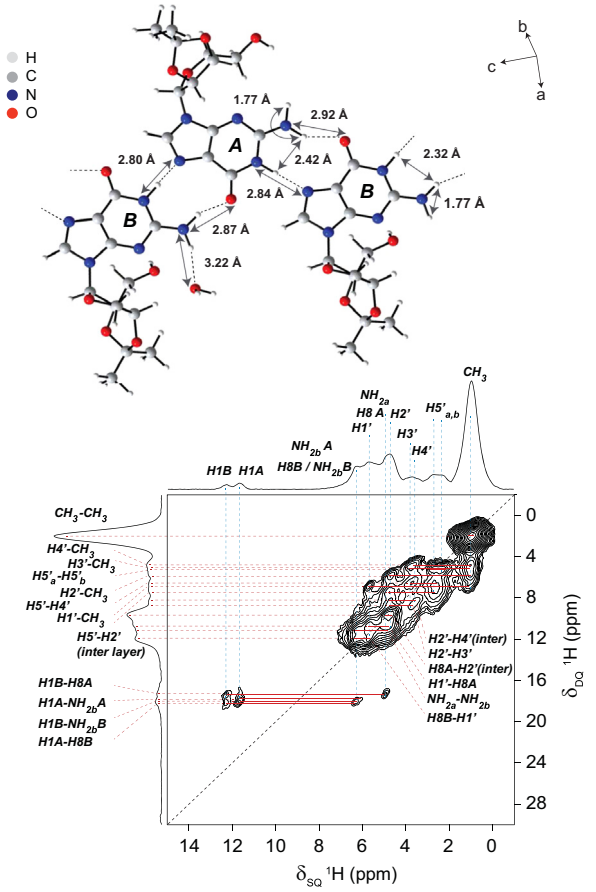

Fig. 6. A ^{1}H (850 MHz) DQ MAS (75 kHz) NMR spectrum, together with skyline projections, of Gace.0.5H_2O, recorded using one rotor period of BABA recoupling. 32 transients were co-added for each of 256 t_1 FIDs (with a rotor-synchronised t_1 increment of 13.3 μs, using the States method to achieve sign discrimination in F_1), corresponding to a total experimental time of 4.6 h. The base contour level is at 0.7% of the maximum peak height. The $F_1 = 2F_2$ diagonal is shown as a dashed line. Horizontal lines (in red) indicate pairs of DQ peaks corresponding to close (< 3.5 Å) H–H proximities. A schematic representation of the crystal structure that identifies intermolecular hydrogen bonding and H–H proximities is shown above the spectra. (For interpretation of the references to colour in this figure legend, the reader is referred to the web version of this article.)

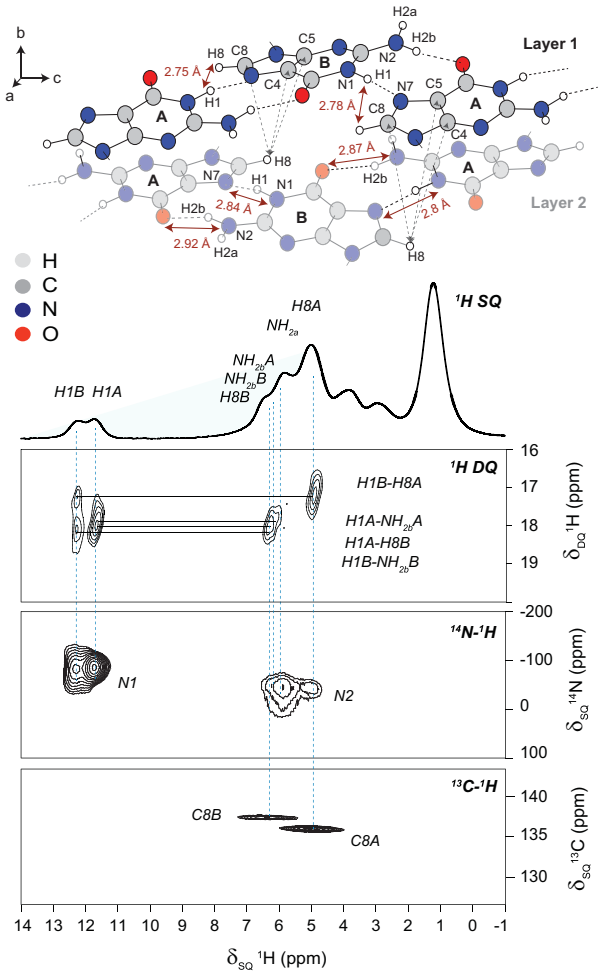

Fig. 7. Spectral regions corresponding to the NH, NH_2 and H8 ^{1}H resonances extracted from (top) ^{1}H (850 MHz, 75 kHz MAS) DQ-SQ (1τ_r of BABA recoupling), (middle) ^{14}N–^{1}H (^{1}H 850 MHz, 75 kHz MAS) HMQC ($\tau_{RCPL} = 12\tau_r = 160$ μs, ^{14}N pulse duration of 5 μs, 128 transients were co-added for each of 48 t_1 FIDs with a rotor-synchronised t_1 increment of 13.3 μs, using the States method to achieve sign discrimination in F_1, corresponding to a total experimental time of 3.4 h) and (bottom) ^{13}C–^{1}H refocused INEPT (^{1}H 500 MHz, 12.5 kHz MAS, eDUMBO-1$_{22}$ ^{1}H homonuclear decoupling, $\tau = \tau' = 1.4$ ms, note that here the horizontal axis corresponds to the F_1 (^{1}H) dimension) two-dimensional NMR spectra of Gace.0.5H_2O. The base contour level is at (top) 1%, (middle) 3% and (bottom) 12% of the maximum peak height. A one-pulse ^{1}H (850 MHz) MAS (75 kHz) MAS spectrum (4 co-added transients) is shown at the top. A schematic representation of the crystal structure that identifies intermolecular hydrogen bonding and CH-π interactions as well as H–H proximities is shown above the spectra.

been rotated as compared to in Fig. 5, i.e., in Fig. 7, the horizontal direction corresponds to the F_1 (^{1}H) dimension. In addition, a one-pulse ^{1}H (850 MHz) MAS (75 kHz) spectrum is presented above the three two-dimensional spectra in Fig. 7. In the schematic representations of the geometry-optimised crystal structures at the top of Figs. 6 and 7, intermolecular NH…*X* hydrogen bonding distances as well as specific H–H proximities are identified.

The ^{14}N–^{1}H HMQC spectrum (Fig. 7, middle) is invaluable for resolving and assigning the NH and NH_2 ^{1}H chemical shifts. Two separate resonances at ^{1}H chemical shifts at 11.6 and 12.3 ppm corresponding to the two distinct NH protons in the asymmetric unit cell are observed. Note that in the GIPAW chemical shift calculations (see Table 3), the higher chemical shift is for molecule B, where as shown in Fig. 6, the NH…N distance is slightly shorter, 2.80 Å as compared to 2.84 Å for molecule A. Considering the ^{14}N–^{1}H HMQC spectrum (Fig. 7, middle) and the ^{1}H–^{13}C refocused INEPT spectral region (Fig. 7, bottom), it is evident that the NH_2 ^{1}H resonances overlap with the H8 ^{1}H resonances. As detailed in Table 4, the interpretation of the ^{1}H DQ MAS spectral region showing cross peaks to the NH1 protons (Fig. 7, top) is complicated by both a close intramolecular proximity with a NH_{2b} proton (at 2.32 and 2.42 Å) and a close intermolecular proximity with a H8 proton (at 2.75 and 2.78 Å), with the NH_{2b} (for both molecules A and B) and H8B resonances observed to overlap. As discussed in Ref. [80], to a good approximation, the relative intensity of DQ peaks at the same SQ frequency depends on the inverse ratio of the internuclear distances to the sixth power, i.e., a DQ peak with a H8 proton is expected to have a relative intensity of ~40% as compared to that of a DQ peak with a NH_{2b} proton.

Table 4
H–H proximities (< 3.0 Å) for the NH1 protons as extracted from the geometry optimised (CASTEP) structure of Gace.0.5H_2O, together with ^{1}H SQ and DQ chemical shifts (see Fig. 7).

Proximity	Molecule	^{1}H–^{1}H distance in Å	^{1}H SQ chemical shifts/ppm	^{1}H DQ chemical shift/ppm
NH1–NH_{2b}	A	2.32	11.6+6.0	17.6
	B	2.42	12.2+6.2	18.4
NH1–H8	A	2.75	11.6+6.3	17.9
	B	2.78	12.2+4.9	17.1

Comparing the experimental and GIPAW calculated ^{1}H chemical shifts in Table 3, it is evident that there are greater discrepancies for the protons bonded to nitrogen than for protons bonded to carbon, notably the calculated NH_{2b} ^{1}H chemical shifts are significantly less than the experimental values. This could be explained by the known temperature dependence of hydrogen-bonded protons, while the GIPAW calculation is performed for a static structure at a temperature of absolute zero [18,81,82]. An alternative explanation is that our sample is not a perfect hemihydrate, but rather, as suggested by the TGA observation in Fig. 2, it is a non-stoichiometric hydrate, with this altering the adopted intermolecular hydrogen bonding; as is evident from Fig. 6, in the hemihydrate crystal structure, one of the NH_{2a} protons forms a relatively weak NH…O hydrogen bond to the water molecule.

4. Summary

This paper has employed an NMR crystallography approach for the characterisation of a self-assembled guanosine derivative whereby experimental multinuclear solid-state NMR spectroscopy (together with powder X-ray diffraction and thermogravimetric analysis) is complemented by GIPAW calculated NMR shieldings. Given the known hygroscopic nature of guanosine itself [83], it is interesting to study a specific hydrated form of a guanosine derivative, namely here a hemihydrate of Gace. There is considerable interest within the context of supramolecular chemistry and pharmaceutical moieties where the solid state NMR methods in association with powder diffraction and computational studies are expected to provide structural and dynamic information on crystal solvates [84–87].

Acknowledgments

Funding from EPSRC (EP/K003674/1) is acknowledged. The UK 850 MHz solid-state NMR Facility used in this research was funded by EPSRC and BBSRC, as well as the University of Warwick including via part funding through Birmingham Science City Advanced Materials Projects 1 and 2 supported by Advantage West Midlands (AWM) and the European Regional Development Fund (ERDF). The powder X-ray diffractometer used in this work was part funded by the Birmingham Science City Advanced Materials Project 1 supported by Advantage West Midlands (AWM) and the European Regional Development Fund (ERDF). This work was performed within the framework of the EPSRC funded Collaborative Computational Project for NMR Crystallography (CCP-NC, EP/J010510/1). Calculations were performed on the University of Warwick Centre for Scientific Computing cluster. We are grateful to Accelrys for providing the Materials Studio Interface for NMR calculations. Helpful discussions with Les Hughes and Helen Blade from AstraZeneca are acknowledged.

References

[1] R.K. Harris, Solid State Sci. 6 (2004) 1025–1037.
[2] R.K. Harris, R.E. Wasylishen, M.J. Duer (Eds.), NMR Crystallography, Wiley, Chichester, 2009.
[3] B. Elena, G. Pintacuda, N. Mifsud, L. Emsley, J. Am. Chem. Soc. 128 (2006) 9555–9560.
[4] C.J. Pickard, F. Mauri, Phys. Rev. B 63 (2001).
[5] J.R. Yates, C.J. Pickard, F. Mauri, Phys. Rev. B 76 (2007).
[6] R.K. Harris, P. Hodgkinson, C.J. Pickard, J.R. Yates, V. Zorin, Magn. Reson. Chem. 45 (2007) S174–S186.
[7] C. Bonhomme, C. Gervais, F. Babonneau, C. Coelho, F. Pourpoint, T. Azais, S.E. Ashbrook, J.M. Griffin, J.R. Yates, F. Mauri, C.J. Pickard, Chem. Rev. 112 (2012) 5733–5779.
[8] J.R. Yates, S.E. Dobbins, C.J. Pickard, F. Mauri, P.Y. Ghi, R.K. Harris, Phys. Chem. Chem. Phys. 7 (2005) 1402–1407.
[9] J.R. Yates, T.N. Pham, C.J. Pickard, F. Mauri, A.M. Amado, A.M. Gil, S.P. Brown, J. Am. Chem. Soc. 127 (2005) 10216–10220.
[10] C. Gervais, R. Dupree, K.J. Pike, C. Bonhomme, M. Profeta, C.J. Pickard, F. Mauri, J. Phys. Chem. A 109 (2005) 6960–6969.
[11] N. Mifsud, B. Elena, C.J. Pickard, A. Lesage, L. Emsley, Phys. Chem. Chem. Phys. 8 (2006) 3418–3422.
[12] L.M. Shao, J.R. Yates, J.J. Titman, J. Phys. Chem. A 111 (2007) 13126–13132.
[13] R.K. Harris, S. Cadars, L. Emsley, J.R. Yates, C.J. Pickard, R.K.R. Jetti, U.J. Griesser, Phys. Chem. Chem. Phys. 9 (2007) 360–368.
[14] E. Zurek, C.J. Pickard, J. Autschbach, J. Am. Chem. Soc. 129 (2007) 4430–4439.
[15] A.C. Uldry, J.M. Griffin, J.R. Yates, M. Perez-Torralba, M.D.S. Maria, A.L. Webber, M.L.L. Beaumont, A. Samoson, R.M. Claramunt, C.J. Pickard, S.P. Brown, J. Am. Chem. Soc. 130 (2008) 945–954.
[16] J.C. Johnston, R.J. Iuliucci, J.C. Facelli, G. Fitzgerald, K.T. Mueller, J. Chem. Phys. 131 (2009) 144503.
[17] E. Salager, G.M. Day, R.S. Stein, C.J. Pickard, B. Elena, L. Emsley, J. Am. Chem. Soc. 132 (2010) 2564–2566.
[18] A.L. Webber, B. Elena, J.M. Griffin, J.R. Yates, T.N. Pham, F. Mauri, C.J. Pickard, A.M. Gil, R. Stein, A. Lesage, L. Emsley, S.P. Brown, Phys. Chem. Chem. Phys. 12 (2010) 6970–6983.
[19] A.L. Webber, L. Emsley, R.M. Claramunt, S.P. Brown, J. Phys. Chem. A 114 (2010) 10435–10442.
[20] L. Stievano, F. Tielens, I. Lopes, N. Folliet, C. Gervais, D. Costa, J.F. Lambert, Cryst. Growth Des. 10 (2010) 3657–3667.
[21] M. Kibalchenko, D. Lee, L.M. Shao, M.C. Payne, J.J. Titman, J.R. Yates, Chem. Phys. Lett. 498 (2010) 270–276.
[22] J.P. Bradley, S.P. Velaga, O.N. Antzutkin, S.P. Brown, Cryst. Growth Des. 11 (2011) 3463–3471.
[23] X. Filip, G. Borodi, C. Filip, Phys. Chem. Chem. Phys. 13 (2011) 17978–17986.
[24] T. Ukmar, V. Kaucic, G. Mali, Acta Chim. Slovenica 58 (2011) 425–433.
[25] A.L. Webber, S. Masiero, S. Pieraccini, J.C. Burley, A.S. Tatton, D. Iuga, T.N. Pham, G.P. Spada, S.P. Brown, J. Am. Chem. Soc. 133 (2011) 19777–19795.
[26] L. Mafra, S.M. Santos, R. Siegel, I. Alves, F.A.A. Paz, D. Dudenko, H.W. Spiess, J. Am. Chem. Soc. 134 (2012) 71–74.
[27] D.C. Apperley, A.S. Batsanov, S.J. Clark, R.K. Harris, P. Hodgkinson, D.B. Jochym, J. Mol. Struct. 1015 (2012) 192–201.
[28] D.C. Apperley, A.F. Markwell, R.K. Harris, P. Hodgkinson, Magn. Reson. Chem. 50 (2012) 680–690.
[29] E. Kucukbenli, K. Sonkar, N. Sinha, S. de Gironcoli, J. Phys. Chem. A 116 (2012) 3765–3769.
[30] F.A. Perras, D.L. Bryce, Angew. Chem., Int. Ed. Engl. 51 (2012) 4227–4230.
[31] M. Sardo, R. Siegel, S.M. Santos, J. Rocha, J.R.B. Gomes, L. Mafra, J. Phys. Chem. A 116 (2012) 6711–6719.
[32] D.V. Dudenko, P.A. Williams, C.E. Hughes, O.N. Antzutkin, S.P. Velaga, S.P. Brown, K.D.M. Harris, J. Phys. Chem. C 117 (2013) 12258–12265.
[33] D.V. Dudenko, J.R. Yates, K.D.M. Harris, S.P. Brown, CrystEngComm 15 (2013) 8797–8807.
[34] M. Baias, C.M. Widdifield, J.N. Dumez, H.P.G. Thompson, T.G. Cooper, E. Salager, S. Bassil, R.S. Stein, A. Lesage, G.M. Day, L. Emsley, Phys. Chem. Chem. Phys 15 (2013) 8069–8080.
[35] M. Baias, J.N. Dumez, P.H. Svensson, S. Schantz, G.M. Day, L. Emsley, J. Am. Chem. Soc. 135 (2013) 17501–17507.
[36] J.T. Davis, Angew. Chem. Int. Edition Engl. 43 (2004) 668–698.
[37] J.T. Davis, G.P. Spada, Chem. Soc. Rev. 36 (2007) 296–313.
[38] S. Lena, S. Masiero, S. Pieraccini, G.P. Spada, Chem.-Eur. J. 15 (2009) 7792–7806.
[39] A. Wong, J.C. Fettinger, S.L. Forman, J.T. Davis, G. Wu, J. Am. Chem. Soc. 124 (2002) 742–743.
[40] G. Wu, A. Wong, Z.H. Gan, J.T. Davis, J. Am. Chem. Soc. 125 (2003) 7182–7183.
[41] R. Ida, G. Wu, Chem. Commun. (2005) 4294–4296.
[42] A. Wong, F.W. Kotch, I.C.M. Kwan, J.T. Davis, G. Wu, Chem. Commun. (2009) 2154–2156.
[43] G. Wu, J.F. Zhu, Prog. Nucl. Magn. Reson. Spectrosc. 61 (2012) 1–70.
[44] T.N. Pham, S. Masiero, G. Gottarelli, S.P. Brown, J. Am. Chem. Soc. 127 (2005) 16018–16019.
[45] T.N. Pham, J.M. Griffin, S. Masiero, S. Lena, G. Gottarelli, P. Hodgkinson, C. Fillip, S.P. Brown, Phys. Chem. Chem. Phys. 9 (2007) 3416–3423.
[46] S.S. Mande, T.P. Seshadri, M.A. Viswamitra, Acta Crystallogr. C 45 (1989) 92–94.
[47] S.P. Brown, Solid State Nucl. Magn. Reson. 41 (2012) 1–27.
[48] B. Elena, A. Lesage, S. Steuernagel, A. Bockmann, L. Emsley, J. Am. Chem. Soc. 127 (2005) 17296–17302.
[49] S.P. Brown, Prog. Nucl. Magn. Reson. Spectrosc. 50 (2007) 199–251.
[50] S. Cavadini, S. Antonijevic, A. Lupulescu, G. Bodenhausen, J. Magn. Reson. 182 (2006) 168–172.
[51] Z.H. Gan, J.P. Amoureux, J. Trebosc, Chem. Phys. Lett. 435 (2007) 163–169.
[52] S. Cavadini, Prog. Nucl. Magn. Reson. Spectrosc. 56 (2010) 46–77.
[53] A.S. Tatton, J.P. Bradley, D. Iuga, S.P. Brown, Z. Phys. Chemie. 226 (2012) 1187–1203.
[54] A.A. Coelho, J. Appl. Crystallogr. 33 (2000) 899–908.
[55] K.D.M. Harris, P.A. Williams, Structure from Diffraction Methods, in: D. Bruce, D. O'Hare, R.I. Walton (Eds.), John Wiley and Sons Ltd, Chichester, 2014.
[56] B.M. Fung, A.K. Khitrin, K. Ermolaev, J. Magn. Reson. 142 (2000) 97–101.
[57] C.R. Morcombe, K.W. Zilm, J. Magn. Reson. 162 (2003) 479–486.
[58] S. Hayashi, K. Hayamizu, Bull. Chem. Soc. Jpn. 64 (1991) 685–687.
[59] G.E. Martin, C.E. Hadden, J. Nat. Prod. 63 (2000) 543–585.

[60] W. Sommer, J. Gottwald, D.E. Demco, H.W. Spiess, J. Magn. Reson. Ser. A 113 (1995) 131–134.
[61] I. Schnell, A. Lupulescu, S. Hafner, D.E. Demco, H.W. Spiess, J. Magn. Reson. 133 (1998) 61–69.
[62] S.P. Brown, H.W. Spiess, Chem. Rev. 101 (2001) 4125–4155.
[63] P.R. Costa, J.D. Gross, M. Hong, R.G. Griffin, Chem. Phys. Lett. 280 (1997) 95–103.
[64] T.G. Oas, R.G. Griffin, M.H. Levitt, J. Chem. Phys. 89 (1988) 692–695.
[65] D. Sakellariou, A. Lesage, P. Hodgkinson, L. Emsley, Chem. Phys. Lett. 319 (2000) 253–260.
[66] B. Elena, G. de Paepe, L. Emsley, Chem. Phys. Lett. 398 (2004) 532–538.
[67] A. Lesage, D. Sakellariou, S. Hediger, B. Elena, P. Charmont, S. Steuernagel, L. Emsley, J. Magn. Reson. 163 (2003) 105–113.
[68] S.J. Clark, M.D. Segall, C.J. Pickard, P.J. Hasnip, M.J. Probert, K. Refson, M.C. Payne, Z. Kristall. 220 (2005) 567–570.
[69] J.P. Perdew, K. Burke, M. Ernzerhof, Phys. Rev. Lett. 77 (1996) 3865–3868.
[70] A. Tkatchenko, M. Scheffler, Phys. Rev. Lett. 102 (2009) 073005.
[71] D. Vanderbilt, Phys. Rev. B 41 (1990) 7892.
[72] J.P. Bradley, C.J. Pickard, J.C. Burley, D.R. Martin, L.P. Hughes, S.D. Cosgrove, S.P. Brown, J. Pharm. Sci. 101 (2012) 1821–1830.
[73] E. Carignani, S. Borsacchi, J.P. Bradley, S.P. Brown, M. Geppi, J. Phys. Chem. C 117 (2013) 17731–17740.
[74] G. Metz, X.L. Wu, S.O. Smith, J. Magn. Reson. Ser. A 110 (1994) 219–227.
[75] A. Lesage, D. Sakellariou, S. Steuernagel, L. Emsley, J. Am. Chem. Soc. 120 (1998) 13194–13201.
[76] R.K. Harris, P. Hodgkinson, T. Larsson, A. Muruganantham, I. Ymen, D.S. Yufit, V. Zorin, Cryst. Growth Des. 8 (2008) 80–90.
[77] R.K. Harris, P. Hodgkinson, V. Zorin, J.N. Dumez, B. Elena-Herrmann, L. Emsley, E. Salager, R.S. Stein, Magn. Reson. Chem. 48 (2010) S103–S112.
[78] J. Czernek, J. Brus, Chem. Phys. Lett. 586 (2013) 56–60.
[79] J. Czernek, J. Brus, Chem. Phys. Lett. 608 (2014) 334–339.
[80] J.P. Bradley, C. Tripon, C. Filip, S.P. Brown, Phys. Chem. Chem. Phys. 11 (2009) 6941–6952.
[81] S.P. Brown, X.X. Zhu, K. Saalwachter, H.W. Spiess, J. Am. Chem. Soc. 123 (2001) 4275–4285.
[82] C.J. Pickard, E. Salager, G. Pintacuda, B. Elena, L. Emsley, J. Am. Chem. Soc. 129 (2007) 8932–8933.
[83] M. Falk, Can. J. Chem. 43 (1965) 314–318.
[84] N. Takata, R. Takano, H. Uekusa, Y. Hayashi, K. Terada, Cryst. Growth Des. 10 (2010) 2116–2122.
[85] K. Fujii, M. Aoki, H. Uekusa, Cryst. Growth Des. 13 (2013) 2060–2066.
[86] D.E. Braun, R.M. Bhardwaj, J.-B. Arlin, A.J. Florence, V. Kahlenberg, U.J. Griesser, D.A. Tocher, S.L. Price, Cryst. Growth Des. 13 (2013) 4071–4083.
[87] A. Bērziņš, E. Skarbulis, T. Rekis, A. Actiņš, Cryst. Growth Des. 14 (2014) 2654–2664.